Composites Science and Technology 181 (2019) 107680

Contents lists available at ScienceDirect

Composites Science and Technology

journal homepage: www.elsevier.com/locate/compscitech

Bio-inspired incorporation of functionalized graphene oxide into carbon nanotube fibers for their efficient mechanical reinforcement

Young-Jin Kim[a,b], Junbeom Park[a], Cheol-Min Yang[a], Hyeon Su Jeong[a], Seung Min Kim[a], Sang Woo Han[b], Beomjoo Yang[c,**], Young-Kwan Kim[a,*]

[a] Institute of Advanced Composite Materials, Korea Institute of Science and Technology, 92 Chudong-ro, Bongdong-eup, Wanju-gun, Jeonbuk, 55324, South Korea
[b] Center for Nanotectonics, Department of Chemistry and KI for the NanoCentury, KAIST, Daejeon, 34141, South Korea
[c] School of Civil Engineering, Chungbuk National University, 1 Chungdae-ro, Seowon-gu, Cheongju, Chungbuk, 28644, South Korea

ARTICLE INFO

Keywords:
Carbon nanotube
Graphene oxide
Surface functionalization
Composite
Fiber

ABSTRACT

An efficient strategy for the enhancement of mechanical properties of carbon nanotube (CNT) fibers is developed using functionalized graphene oxide with a quaternary ammonium (QA) group (QA-FGO). QA-FGO is designed to induce the π-cation interaction, one of the strongest interactions in living systems, with CNT fibers. Based on the strategy, the tensile strength (58 MPa), specific strength (0.49 N/tex), modulus (2.5 GPa) and toughness (1.1 MJ/m^3) of CNT fibers are enhanced to 409 MPa, 0.65 N/tex, 13.4 GPa, and 10.1 MJ/m^3, respectively. The reinforcement mechanism is systematically demonstrated with experimental and theoretical approaches.

1. Introduction

Carbon nanotubes (CNTs) have been considered one of the promising materials to develop next-generation high-performance fibrous materials owing to their outstanding chemical inertness, thermal, mechanical, and electrical properties [1]. There have been many attempts to produce a CNT fiber to fully reenact the intrinsic properties of individual CNTs for practical applications that require extreme properties (in automobile, electric transmission, defense, and aerospace industries) [2]. Several spinning techniques of CNTs have been developed and they can be categorized into direct spinning from chemical vapor deposition with floating catalysts [3], liquid crystal spinning from highly concentrated CNT dope in super acids [4], and forest spinning from vertical arrays of CNT on a substrate [5].

Regarding the large-scale and continuous production, the direct spinning process is highly desirable but has suffered from relatively inferior mechanical properties of individual CNTs [6]. This problem is not restricted to directly-spun CNT fibers but to all CNT fibers. The problem stems from the combined effects of poor packing density and weak interfacial shear strength between individual CNTs consisting of CNT fibers. The packing density and interfacial shear strength of CNT fibers should be enhanced to improve their mechanical properties, and thus several approaches have been developed such as densification with liquids [7] or super acids [8], polymer [9] or chemical vapor infiltration [10], acid treatment [11], or roll-to-roll pressing [12]. Incorporation of graphene derivatives is another interesting strategy that can provide new functions to CNT fibers and reinforce their mechanical properties [13,14]. The criteria for efficient reinforcement of CNT fibers include the following: (i) improvement of the interfacial shear strength between individual CNTs, (ii) densification to minimize the voids in CNT fibers, and (iii) no structural damage to individual CNTs consisting of CNT fibers.

Recently, Wang et al. improved the interfacial shear strength of CNT fibers and the mechanical properties of CNT fibers using a nano-sized graphene oxide (GO) that penetrated the CNT fiber and improved the interfacial shear strength of the CNT fiber [14]. They only emphasized the size effect of the GO on reinforcement by efficient penetration and interlocking through its oxygenated functional groups with a large interfacial area. However, the functional groups of GO derivatives can also play an important role in the reinforcement of CNT fibers because they directly affect the interfacial shear strength between GO derivatives and CNT fibers through their chemical interactions. In addition, the incorporation of GO derivatives into CNT fibers can improve the applicability of CNT fibers as well as the interfacial shear strength. For examples, Hua et al. showed that the coating of amine-functionalized glass fiber surfaces with GO and CNTs through a simple physical-chemical method lead to the enhancement of wettability of the glass fibers with epoxy droplets and then improvement of fiber-matrix interfacial

* Corresponding author.
** Corresponding author.
E-mail addresses: byang@cbnu.ac.kr (B. Yang), youngkwan@kist.re.kr (Y.-K. Kim).

https://doi.org/10.1016/j.compscitech.2019.107680
Received 16 January 2019; Received in revised form 4 June 2019; Accepted 8 June 2019
Available online 09 June 2019

bond property with a high synergistic effect [15]. Pan et al. reported that the fabrication of hybrid films composed of reduced GO and multi-walled CNT (rGO/MWCNT) through vacuum filtration followed by the hydrothermal reduction process [16]. The rGO/MWCNT hybrid films exhibited high flexibility and thermal conductivity with a great anisotropic thermal properties. Those previous reports suggested that the high potential of incorporation of GO derivatives into CNT fibers for the various applications including fiber-reinforced composites and thermal management.

In this regard, the rational design of chemical interactions at interfaces is a prerequisite to efficiently reinforcing the CNT fibers using GO derivatives but the functional group effect of GO derivatives on the mechanical reinforcement has not been demonstrated. For the rational design of a strongly interactive interface, mimicking natural adhesive materials such as mussel-foot proteins can be an effective way [17]. Especially, π-cation interactions [18], one of the main driving forces for adhesiveness of mussel proteins, are quite promising because they are much stronger than hydrogen bonding and electrostatic interactions [19].

In this study, we investigate the functional group effect of GO on the enhancement of mechanical properties of CNT fibers using functionalized GO (FGO) to harness the π-cation interactions (Fig. 1). A quaternary ammonium (QA) functionalized GO (QA-FGO) was synthesized and then utilized as an interlocking agent for CNT fibers. Density functional theory (DFT) and molecular dynamics (MD) simulations were employed to reveal the interactions of GO and QA-FGO with CNT fibers and the mechanical behavior of the resulting interlocked CNT fibers. Experimental and theoretical results demonstrated that the incorporation of QA-FGO into CNT fibers resulted in more efficient reinforcement of their mechanical properties than pristine GO through the stronger chemical interaction. The tensile strength (58 MPa), specific strength (0.49 N/tex), modulus (2.5 GPa), and toughness (1.1 MJ/m^3) of CNT fibers were considerably enhanced by the incorporation of QA-FGO to 409 MPa, 0.65 N/tex, 13.4 GPa, and 10.1 MJ/m^3, respectively.

2. Experimental section

2.1. Direct spinning of CNT fibers

CNT fibers were directly spun from the chemical vapor deposition (CVD) reactor with floating catalysts [3,10]. Acetone (97.9 wt%, carbon source), ferrocene (1.2 wt%, catalyst source), and thiophene (0.9 wt%, promotor source) were continuously injected into the CVD reactor as hydrogen and argon-carrier gas (2000 sccm) were injected into a hot furnace (1200 °C) through a controlled evaporation mixer and a pre-heater. All injection lines were heated to 100 °C to prevent re-condensation of the reactants in the vapor phase. The injected reactants were thermally decomposed in hot furnace (1170 °C), and Fe nanoparticles were formed by agglomeration of detached Fe atoms from ferrocene. Then, carbon from acetone dissolved in Fe nanoparticles, and sulfur from thiophene decreased the solubility of carbon in Fe nanoparticles to lower the saturation concentration of carbon. After the saturation, dissolved carbon atoms were extracted as form of graphitic layer and finally CNTs grew from those nanoparticles. The grown CNTs formed the hollow and entangled intermediate structure (usually called CNT sock) and flowed to bottom of furnace. Water bath was located at the bottom of furnace in order to seal the exhaust gas and the CNT sock was pulled out through the water bath. The CNT sock was shrunk into fibrous form at the surface of water due to CNT's hydrophobicity.

2.2. Synthesis of GO and QA-FGO

GO was synthesized by the previously reported process [20]. For the

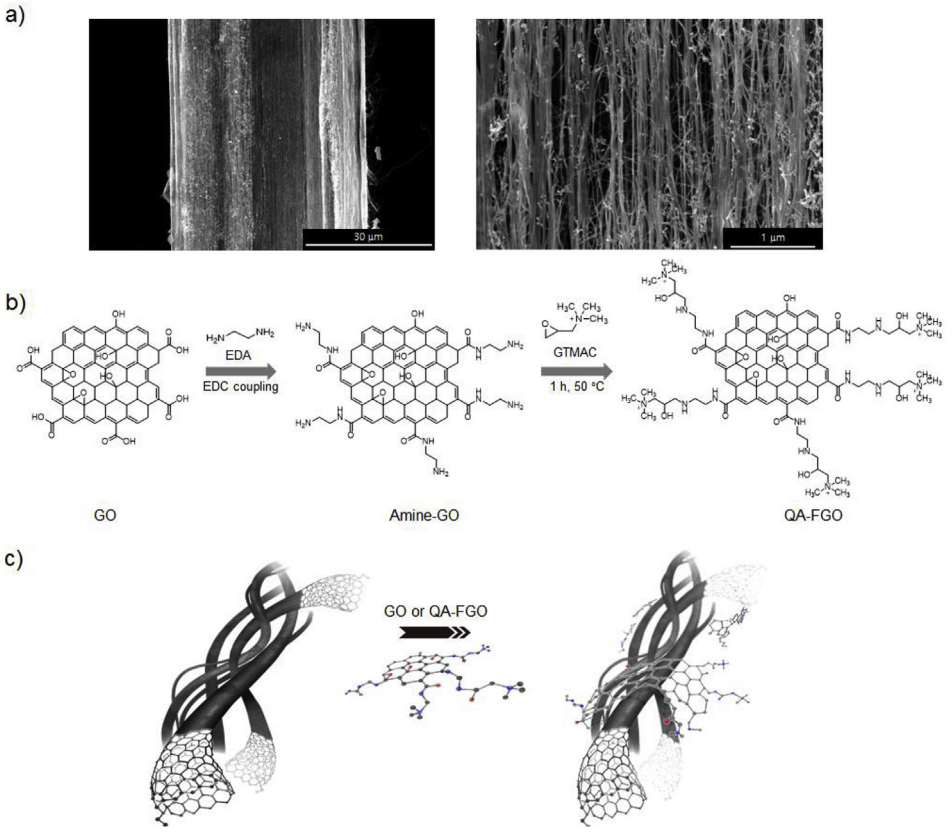

Fig 1. a) SEM images of spun CNT fibers with different magnifications, (b) synthetic process of QA-FGO, and (C) schematic diagram of incorporation of GO derivatives into CNT fibers.

synthesis of QA-FGO, a two-step surface functionalization process (amination of GO and subsequent modification of amine into the QA group) was employed. First, 10 mg of GO was dispersed in 20 mL of water by sonication until there is no visible particle. Then, 400 mg of 1-ethyl-3-(3-dimethylaminopropyl)carbodiimide (EDC) and 5 mL of ethylene diamine were added to the GO suspension (0.5 mg/mL), and the mixture was stirred for 12 h under ambient conditions [21]. The amine-functionalized GO was obtained by dialysis against water for 4 d. Then, 1.2 g of NaOH and 1.5 g of glycidyltrimethylammonium chloride were added to 20 mL of the aminated GO suspension (0.5 mg/mL). Finally, the resulting mixture was heated to 60 °C, stirred for 2 h under ambient conditions, and purified by repeated centrifugation and washing five times to collect QA-FGO.

2.3. Interlocking of CNT fibers with GO and QA-FGO

The synthesized GO and QA-FGO were dispersed in water (0.05 mg/mL). *N,N*-dimethylformamide (DMF) was added to the 10 mL of GO and QA-FGO aqueous suspensions, respectively, where the volume ratio of water to DMF was 98:2. Then, CNT fibers were immersed in the prepared solutions to interlock pristine CNT fibers with GO or QA-FGO. After the reaction, reinforced CNT fibers were washed with water and ethanol and dried under vacuum at room temperature for 1 h. As a control, CNT fibers were immersed into pure DMF, washed with water and ethanol, and dried under vacuum to reveal the effect of wet-chemical processes on their structure and mechanical properties.

2.4. Characterization of tensile strength

Each CNT fiber was cut to 30 mm pieces for the tensile test. Mechanical properties of CNT fibers were measured using the Textechno Favimat instrument. Loading rate and gauge length were 2 mm/min and 20 mm, respectively. At least five samples were tested to obtain a uniform value.

2.5. DFT calculations

DFT calculations of CNT, GO, and QA-FGO were performed using the quantum chemical module of DMol3 that is a part of the Material Studio 2017 developed by BIOVIA Corporation [22]. DMol3 uses localized numerical orbitals for the basis functions and can be used to predict the energy and structure of atoms without experimental input [23]. The energy of structures was calculated with the Becke-Lee-Yang-Parr functional of the generalized gradient approximation and double-numeric plus polarization. The DMol3 code with a smearing of 0.005 Ha was applied to improve the computational performance. The density was mixed as 0.2 charge and 0.5 spin, respectively. The electrostatic potential (ESP) was obtained by analyzing the calculation results.

2.6. MD simulations

An enhancement mechanism of the present heterogeneous fibers was examined using MD simulations. The original size of the CNT fibers is too large to be calculated by MD simulations; thus, the molecular structure of the representative volume element (RVE) was considered in this study [24,25]. For practical calculations, the initial configuration of CNT fibers was assumed to be four CNTs (diameter = 7.2 Å, length = 32 Å) within a 32 × 32 × 58.5 $Å^3$ cell as the RVE. Twenty-five GO and QA-FGO molecules were then randomly inserted into the RVE system. To reduce the influence of the increase in density on the calculation results, an additional four CNTs were added to the existing RVE. To equilibrate the system, geometry optimization, the constant-temperature/constant-volume ensemble (NVT), and constant-temperature/constant-pressure ensemble (NPT) simulations were conducted using the Forcite module in the package Material Studio 2017. Geometry optimization was carried out using the Smart algorithm until a specified convergence tolerance was obtained. The convergence tolerance of the force, displacement, and energy were set to be 0.001 kcal/mol/Å, 1.0^{-5}, and 2.0^{-5} kcal/mol, respectively. The NVT dynamics were then performed for 2 ns at 1 atm and 300 K using the Nosé-Hoover thermostat. The time-steps for the dynamics were 1 fs and trajectories with 5 ps intervals were set to perform the analysis. The atom-based method and Ewald summation were applied to describe the van der Waals and long-range Coulomb interactions [26]. Based on the equilibrated cell information calculated with previous NVT simulations, NPT dynamics were carried out additionally until the system reached the equilibrium state [27]. The identical non-bond and thermostat conditions as NPT simulations were applied to the NVT dynamics. All calculations were carried out based on the Condensed-phase Optimized Molecular Potentials for Atomistic Simulation Studies force field [28,29].

2.7. Characterization

Raman spectra of GO and CNT fibers were obtained using a HORIBA LabRAM instrument (Jobin Yvon, France) with an operating wavelength of 514 nm using an air-cool He/Ne laser. The SEM images of GO and CNT fibers were observed using a NOVA NanoSEM 450 instrument (FEI company, Netherlands). Fourier transform infrared (FT-IR) analysis was carried out using a Nicolet iN10 microscope (Thermo Scientific, USA) in a reflective mode. The cross-sectional areas were measured by cutting the CNT fibers with a Helios NanoLab 650 dual-beam focused ion beam (FEI company, Netherlands) and then divided by the cosine of the tilted angle (90°–30°). The zeta potential of GO and QA-FGO was analyzed using a Nano ZS analyzer (Malvern, UK). X-ray photoelectron spectroscopy (XPS) spectra were obtained using a Thermo Scientific K-alpha instrument (Thermo VG, USA) under a high vacuum condition (10^{-7}–10^{-9}). Transmission electron microscopy (TEM) images of CNT fibers were examined by using a Tecnai (G2 S-Twin, FEI) with a field emission gun operating at 200 kV and a Oneview camera (Gatan) for imaging and structural analysis.

3. Results and discussion

The pristine CNT fibers were produced using the direct spinning process with a floating catalyst CVD (FC-CVD) reaction with continuous feeding of gaseous acetone (carbon source), ferrocene (catalyst precursor), and thiophene (promotor precursor) into the vertical CVD reactor, respectively [10]. The direct spun CNT fibers were composed of double-walled CNTs with a diameter range of 2–3 nm (Fig. S1). The produced CNT fibers exhibited a complicated hierarchical structure with numerous voids and their porous structure resulted in inefficient load transfer and then inferior mechanical properties to individual CNTs (Fig. 1a). Therefore, the load transfer efficiency between the CNT bundles consisting of CNT fibers should be enhanced to improve their mechanical properties. To enhance the interfacial-shear strength of CNT fibers, CNT fibers were treated with GO derivatives with different functional groups as interlocking agents. We synthesized GO [20], aminated it using EDC coupling reactions with ethylene diamine (amine-GO) [21], and finally converted the amine groups into a quaternary ammonium group (QA-FGO) for a clear demonstration of their functional group effect on the reinforcement of CNT fibers (Fig. 1b).

The morphology of GO, amine-FGO, and QA-FGO was examined using SEM. The lateral dimensions of GO, amine-FGO, and QA-FGO sheets were ~3 μm (Fig. S2a in the supporting information). This result suggests that GO, amine-FGO, and QA-FGO sheets possess an analogous lateral dimension and thus GO sheets are not cleaved during the sequential surface functionalization reactions. To confirm the successful functionalization, the chemical structure changes of GO during the sequential surface functionalization reactions were investigated with XPS analysis. The XPS results showed that GO was successfully functionalized with QA groups by our experimental processes (Fig. S2 b, c). The

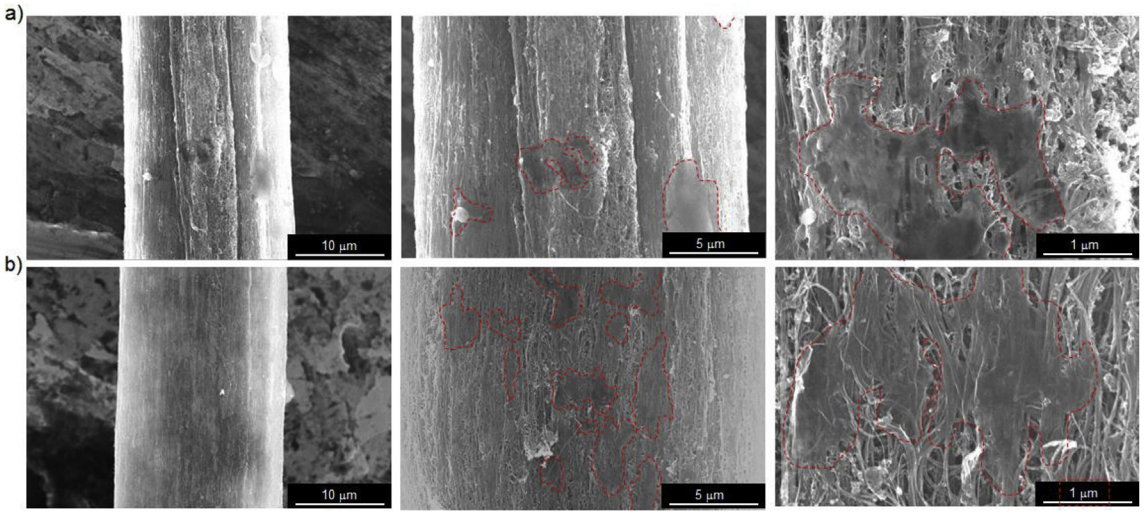

Fig. 2. a) SEM images of GO@CNT and (b) QA-FGO@CNT fibers with different magnifications.

detailed XPS analysis of C and N 1s spectra such as binding energy positions, full width of half maximums and compositions of each chemical bond were provided in Figs. S3 and S4 as tables, respectively. For further confirmation of QA functionalization of GO, GO, amine-FGO and QA-FGO were characterized by using FT-IR and Raman spectroscopic (Fig. S5). All of those spectroscopic results indicated GO was successfully converted into QA-FGO (for pH dependent zeta potential values of amine-FGO and QA-FGO, see Fig. S6). The synthesized GO and QA-FGO were then incorporated into CNT fibers to systematically investigate their influence on the mechanical properties of CNT fibers. The sequential processes of GO and QA-FGO synthesis and their incorporation into the CNT fibers are shown in Fig. 1c. SEM images clearly show that GO and QA-FGO are immobilized on the outer surface of CNT fibers but their surface coverage of CNT fibers is different from each other (Fig. 2). Although GO and QA-FGO sheets were also attached on the outer surface of CNT fibers owing to their larger size than porous structure of CNT fibers (Fig. 2), the surface coverage of QA-FGO sheets was relatively higher than GO sheets on CNT fibers (Fig. 2). The SEM characterization results support our hypothesis that QA-FGO sheets possess higher interaction energy than GO based on the strong π-cation interaction.

Raman spectroscopy was carried out to examine the changes in the sp^2 carbon structure of CNT, GO incorporated CNT (GO@CNT), and QA-FGO incorporated CNT (QA-FGO@CNT) fibers. CNT fibers exhibited typical D- and G-peaks at 1344 cm^{-1} and 1575 cm^{-1} [10]. The I_G/I_D value was measured to be 19.5 ± 0.3, which implies that the CNT fibers possess well-ordered sp^2 carbon structures (Fig. 3). After the incorporation of GO and QA-FGO sheets, GO@CNT fibers showed a decreased I_G/I_D value of 11.7 ± 3.7 and the value of QA-FGO@CNT fibers was measured to be 8.6 ± 1.5 (Fig. 3). The decreased I_G/I_D values of GO@CNT and QA-FGO@CNT fibers compared to CNT fibers resulted from the immobilization of GO and QA-FGO sheets that have the structures highly defected by sequential oxidation, exfoliation, and functionalization processes of natural graphite [30]. Considering the analogous I_G/I_D values of GO and QA-GO (Fig. S3b), the higher I_G/I_D value of the GO@CNT fiber than the QA-FGO@CNT fiber implies that QA-FGO sheets provide a higher surface immobilization density on CNT fibers than GO sheets. The results agree with the SEM results. Importantly, the 2D band of CNT fibers was up-shifted from 2668 cm^{-1} to 2681 and 2691 cm^{-1} by incorporation of GO and QA-FGO, respectively (Fig. 3). This up-shift was attributed to the π-π and π-cation interactions between GO derivatives and CNT fibers [31] and the higher up-shift on QA-FGO@CNT fiber than GO@CNT fiber clearly indicated that QA-FGO has stronger interaction with CNT fiber than GO through the π-cation interaction.

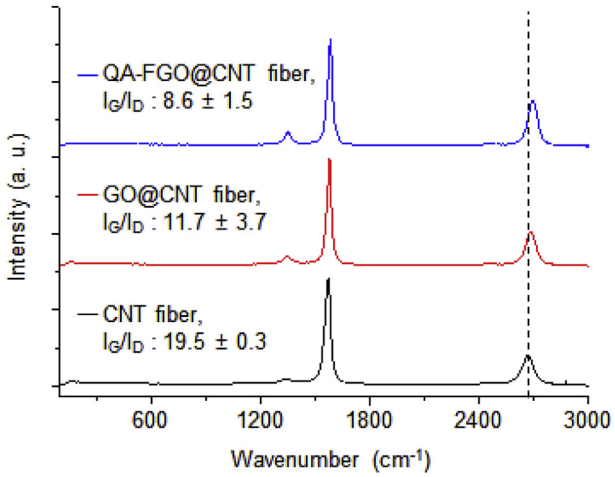

Fig. 3. Raman spectra of CNT, GO@CNT, and QA-FGO@CNT fibers.

Mechanical properties of CNT, GO@CNT, and QA-FGO@CNT fibers were investigated to confirm the reinforcement of CNT fibers by GO and QA-FGO incorporation (Fig. 4). The tensile strength, modulus, toughness, and specific tensile strength of CNT fibers were measured to be 58 MPa, 2.5 GPa, 1.1 MJ/m^3, and 34 cN/tex and after the incorporation of GO, those mechanical properties were considerably enhanced to 315 MPa, 9.6 GPa, 7.5 MJ/m^3, and 55 cN/tex, respectively (Fig. 4). This enhancement implies that despite its large lateral size, the direct adsorption of GO sheets on the outer surface of CNT fibers can reinforce their mechanical properties. Previous studies reported that the incorporation of large GO sheets over approximately 100 nm in their lateral dimension did not induce mechanical reinforcement of CNT fibers owing to the inefficient penetration into the voids of CNT fibers [17]. Although the lateral dimension of GO sheets used in this study was ~3 μm, the mechanical properties of CNT fibers were greatly enhanced. Previous studies did not provide detailed information on the chemical structure of GO [13,14], but our results suggest that the chemical structure of GO is one of the most important factors for the reinforcement of CNT fibers. Compared to the GO@CNT fibers, the QA-FGO@CNT fibers exhibited higher mechanical properties such as tensile strength (409 MPa), modulus (13.4 GPa), toughness (10.1 MJ/m^3), and specific tensile strength (64 cN/tex) (Fig. 4). The higher reinforcement effect of QA-FGO than that of GO further supported our hypothesis that the functional groups of GO derivatives greatly influence the

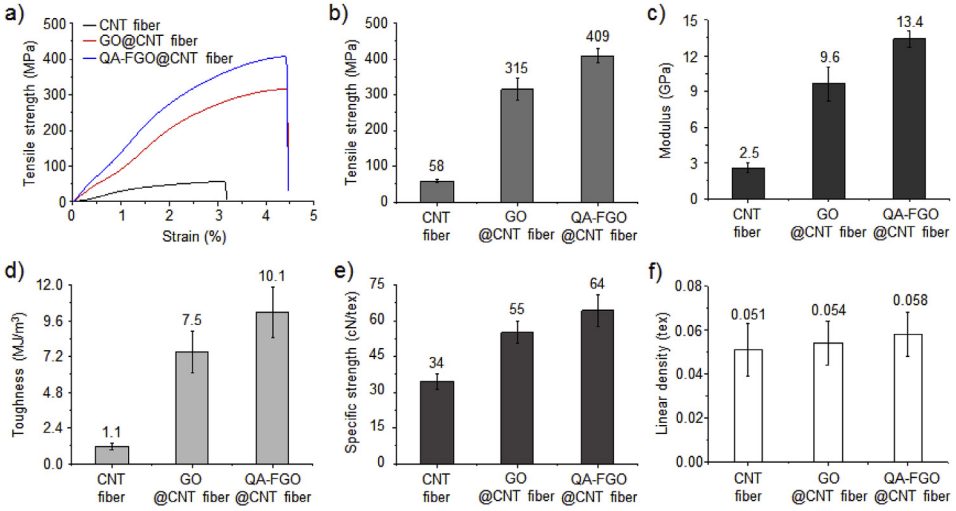

Fig. 4. a) Stress-strain curves, tensile strength, (b) modulus, (c) toughness, (d) specific tensile strength, and linear density of CNT, GO@CNT, and QA-FGO@CNT fibers.

reinforcement efficiency of CNT fibers. In addition, their linear density increased in the order of CNT, GO@CNT and QA-FGO@CNT fibers (Fig. 4f). The increasing linear density of CNT fibers implies that GO derivatives are more incorporated into CNT fibers and thus the functional groups of GO derivatives significantly affect the incorporation/reinforcement efficiency of CNT fibers. These results agree with the SEM and Raman spectroscopic characterization results (Figs. 2 and 3), which show that QA-FGO sheets have higher surface coverage on CNT fibers than GO sheets. The affinity of QA-FGO to CNT fibers originates from the strong π-cation interaction between the QA-FGO and CNT fibers. As a control, CNT fibers were immersed in pure DMF without GO and QA-FGO, washed, and dried under the equivalent conditions for their reinforcement experiment with GO and QA-FGO sheets. The resulting CNT fibers exhibited an analogous hierarchical structure and mechanical properties with pristine CNT fibers (Fig. S7). These results demonstrate that the enhanced mechanical properties of CNT fibers are derived from the incorporation of GO and QA-FGO sheets.

Cross-sectional analysis of CNT, GO@CNT, and QA-FGO@CNT fibers was carried out to reveal the incorporation effect of GO and QA-FGO on the density of CNT fibers. The cross-sectional SEM images of CNT fibers exhibited their loosely-packed porous structure (Fig. 5a). However, the porous structure of CNT fibers was densified with the incorporation of GO (Fig. 5b) and the degree of densification increased with the incorporation of QA-FGO (Fig. 5c). These results imply that the densification effect of GO derivatives is also closely related to their surface functional groups. Since QA-FGO sheets can form π-cation interactions with CNT fibers, the QA-FGO@CNT fibers exhibit more densification effect and enhanced mechanical properties than GO@CNT fibers. The functionalization of GO sheets with QA groups lead to an efficient mechanical reinforcement of CNT fibers through the formation of a bio-inspired strongly interactive interface. By contrast, the cross-sectional structure of pristine CNT fibers were not noticeably changed after the sequential processes including incubation in pure DMF, washing with water and ethanol, and drying under vacuum (Fig. S8). The procedure was equal to the processes to incorporate GO derivatives into CNT fibers except presence of GO derivatives in DMF. This result clearly demonstrated that the densification effect of CNT fibers were derived from the incorporation of GO and QA-FGO onto their surfaces.

For theoretical investigation of interfacing structures between GO derivatives and CNT fibers, the ESP maps of CNT, GO, and QA-FGO were constructed using the DMol3 module (Fig. 6a). The CNT is negatively charged on its overall outer surface compared to its upper and lower ends, but GO is negatively charged along its edge owing to the carboxylic acid groups (Fig. 6a). In contrast, QA-FGO is positively

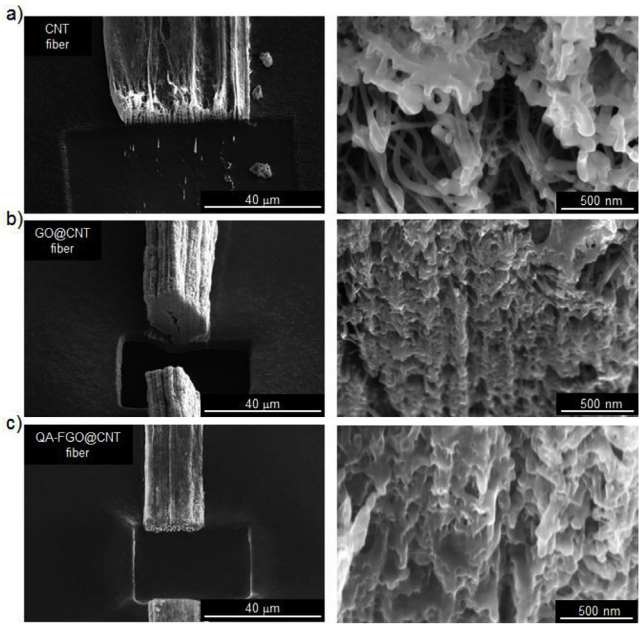

Fig. 5. Low and high magnified cross-sectional SEM images of (a) CNT, (b) GO@CNT, and (c) QA-FGO@CNT fibers.

charged along its edge because carboxylic acid groups are converted into QA groups. Different ESP values can greatly affect the mechanical behavior of CNT fibers when they are utilized as interlocking materials [32]. The main reasons of the inferior mechanical properties of CNT fibers to those of individual CNTs are low interfacial shear strength between CNTs through Van der Walls forces and the loosely-packed structure of CNTs. Therefore, the interlocking materials for CNT fibers should have strong interactions with CNTs to efficiently enhance their interfacial-shear strength. Based on their EST maps, GO cannot have strong interactions with CNT fibers owing to their negatively charged surfaces, but QA-FGO can strongly interact with CNT fibers through electrostatic interactions between positive charges of QA-FGO and π-electrons of CNT fibers (Fig. 6a).

To further explain the energy of the interaction of GO and QA-FGO with CNT fibers, the interaction energies of CNT, GO@CNT, and QA-FGO@CNT fibers were calculated through MD simulations (Fig. 6b). Although RVE models in this simulation are ideal systems that may be different from the real systems, these simulations can indirectly predict

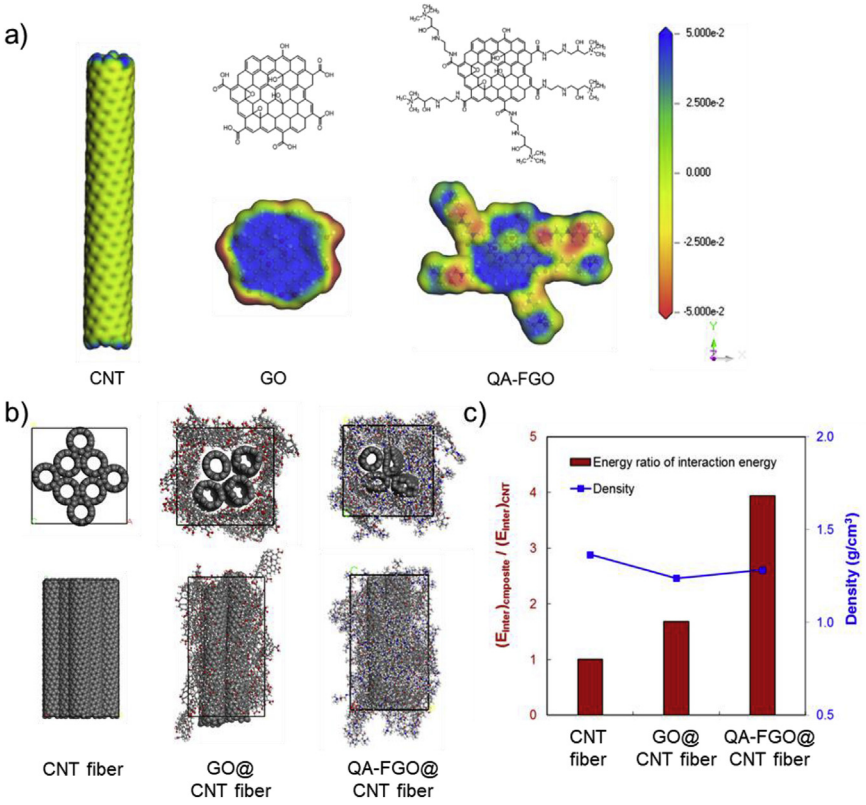

Fig. 6. a) Chemical structures and ESP maps of CNT, GO, and QA-FGO. b) Final atomistic structures of RVE models and (c) interaction energy and density of CNT, GO@CNT, and QA-FGO@CNT fibers calculated with MD simulations.

the mechanical behavior of CNT, GO@CNT, and QA-FGO@CNT fibers and improve the understanding of the enhancement mechanism. The interaction energy between the CNT fibers and additives can be calculated using the following equation [33,34].

$$E_{\text{interaction}} = E_{\text{total}} - E_{\text{CNT}} - E_{\text{addtive}}$$

where E_{total} is the total energy of the systems, E_{CNT} and E_{additive} are the potential energies of four core CNTs in the center (a model of CNT fibers) and surrounding substances (the outer CNTs, GO, and QA-FGO), respectively. The interaction energy was calculated to be high in the order of QA-FGO@CNT, GO@CNT, and CNT fibers (Fig. 6c), consistent with the results of the tensile test, which show that QA-FGO has a higher enhancement effect than GO for CNT fibers (Fig. 4). By contrast, the density of CNT fibers was calculated to be the highest and QA-FGO@CNT fiber was predicted to possess slightly higher density than GO@CNT fiber. These results imply that the differences in energy levels in the models of CNT, GO@CNT, and QA-FGO@CNT systems originate from their different interactions caused by their chemical structures rather than physical densities (Fig. 6c). Simulation results show that the mechanical reinforcement effect of CNT fibers by the incorporation of GO and QA-FGO is derived from their chemical interactions and that QA-FGO has a stronger interaction with CNT fibers than GO owing to its positively charged QA functional groups. Detailed information on the interaction energy calculation and the expected stress-strain curves of CNT, GO@CNT, and QA-FGO@CNT fibers is provided in Figs. S9 and S10, respectively. Additionally, to better understand the densification effect of QA-FGO, MD simulation with respect to time was performed, as shown in Figs. S11 and S12. MD simulation results showed that CNT fibers were gradually surrounded with GO and QA-FGO with flat morphology at initial state, and the morphology of GO and QA-FGO became curved along with the surface of CNT fibers over time. Then, stabilization of the material was achieved with distorted shape of CNTs induced by conformal contacts between GO derivatives and CNT fibers through their attractive interaction. As a result, entire CNT fiber was densified homogenously on the microstructure by using GO derivatives. As expected, QA-FGO induced much higher distortion of CNTs than GO, and thus we can confirm that QA-FGO sheets exhibited more densification effect than GO sheets owing to the higher attractive interaction of QA-FGO sheets with CNT fibers than GO sheets.

4. Conclusion

The incorporation of QA-FGO into CNT fibers resulted in an efficient mechanical reinforcement of CNT fibers through harnessing bio-inspired strongly interactive interfaces. QA-FGO was synthesized by sequential conjugation reactions on GO and then incorporated into CNT fibers by π-cation, π-π, and van der Walls interactions. By the bio-inspired combinatorial interactions, the tensile strength (58 MPa), specific strength (0.49 N/tex), modulus (2.5 GPa), and toughness (1.1 MJ/m^3) of CNT fibers were increased to 409 MPa, 0.65 N/tex, 13.4 GPa, and 10.1 MJ/m^3, respectively. To analyze the mechanical enhancement mechanism, we carried out DFT calculations and MD simulations. The ESP maps of CNT, GO, and QA-FGO and the simulation results provide an insight into the correlations between electrostatic interactions and the mechanical behavior of CNT, GO@CNT, and QA-FGO@CNT fibers. Further analyses of MD simulations revealed that those chemical structures of the GO derivatives have a significant effect on the increase in the interaction energy. The results of this study are valuable for the design of a strongly interactive interface for development of a high-performance CNT fiber and for potential applications of CNT fibers.

Notes

The authors declare no competing financial interest.

Acknowledgements

This research was financially supported by grants from the Korea Institute of Science and Technology Open Research Program (ORP) and Nano Material Technology Development Program through the National Research Foundation of Korea funded by the Ministry of Science, ICT and Future Planning (2016M3A7B4027223) and (2016M3A7B4905619).

Appendix A. Supplementary data

Supplementary data to this article can be found online at https://doi.org/10.1016/j.compscitech.2019.107680.

References

[1] M. Dresselhaus, G. Dresselhaus, J.-C. Charlier, E. Hernandez, Electronic, thermal and mechanical properties of carbon nanotubes, Phil. Trans. Roy. Soc. Lond. 362 (2004) 2065–2098.
[2] N. Behabtu, M.J. Green, M. Pasquali, Carbon nanotube-based neat fibers, Nano Today 3 (2008) 24–34.
[3] K. Koziol, J. Vilatela, A. Moisala, M. Motta, P. Cunniff, M. Sennett, A. Windle, High-performance carbon nanotube fiber, Science 318 (2007) 1892–1895.
[4] D.E. Tsentalovich, R.J. Headrick, F. Mirri, J. Hao, N. Behabtu, C.C. Young, M. Pasquali, Influence of carbon nanotube characteristics on macroscopic fiber properties, ACS Appl. Mater. Interfaces 9 (2017) 36189–36198.
[5] M. Zhang, K.R. Atkinson, R.H. Baughman, Multifunctional carbon nanotube yarns by downsizing an ancient technology, Science 306 (2004) 1358–1361.
[6] S. Boncel, R.M. Sundaram, A.H. Windle, K.K. Koziol, Enhancement of the mechanical properties of directly spun CNT fibers by chemical treatment, ACS Nano 5 (2011) 9339–9344.
[7] J. Qiu, J. Terrones, J.J. Vilatela, M.E. Vickers, J.A. Elliott, A.H. Windle, Liquid infiltration into carbon nanotube fibers: effect on structure and electrical properties, ACS Nano 7 (2013) 8412–8422.
[8] H. Cho, H. Lee, E. Oh, S.-H. Lee, J. Park, H.J. Park, S.-B. Yoon, C.-H. Lee, G.-H. Kwak, W.J. Lee, Hierarchical structure of carbon nanotube fibers, and the change of structure during densification by wet stretching, Carbon 136 (2018) 409–416.
[9] Y. Jung, T. Kim, C.R. Park, Effect of polymer infiltration on structure and properties of carbon nanotube yarns, Carbon 88 (2015) 60–69.
[10] J. Lee, T. Kim, Y. Jung, K. Jung, J. Park, D.-M. Lee, H.S. Jeong, J.Y. Hwang, C.R. Park, K.-H. Lee, S.M. Kim, High-strength carbon nanotube/carbon composite fibers via chemical vapor infiltration, Nanoscale 8 (2016) 18972–18979.
[11] T.Q. Tran, Z. Fan, A. Mikhalchan, P. Liu, H.M. Duong, Post-treatments for multifunctional property enhancement of carbon nanotube fibers from the floating catalyst method, ACS Appl. Mater. Interfaces 8 (2016) 7948–7956.
[12] J. Wang, X. Luo, T. Wu, Y. Chen, High-strength carbon nanotube fibre-like ribbon with high ductility and high electrical conductivity, Nat. Commun. 5 (2014) 3848.
[13] F. Meng, J. Zhao, Y. Ye, X. Zhang, S. Li, J. Jia, Z. Zhang, Q. Li, Multifunctionalization of carbon nanotube fibers with the aid of graphene wrapping, J. Mater. Chem. 22 (2012) 16277–16282.
[14] Y. Wang, G. Colas, T. Filleter, Improvements in the mechanical properties of carbon nanotube fibers through graphene oxide interlocking, Carbon 98 (2016) 291–299.
[15] Y. Hua, F. Li, G.-W. Huang, H.-M. Xiao, Y.-Q. Li, N. Hu, S.-Y. Fu, Positive synergistic effect of graphene oxide/carbon nanotube hybrid coating on glass fiber/epoxy interfacial normal bond strength, Compos. Sci. Technol. 149 (2017) 294–304.
[16] T.-W. Pan, W.-S. Kuo, N.-H. Tai, Tailoring anisotropic thermal properties of reduced graphene oxide/multi-walled carbon nanotube hybrid composite films, Compos. Sci. Technol. 151 (2017) 44–51.
[17] L. Hamming, X. Fan, P. Messersmith, L. Brinson, Mimicking mussel adhesion to improve interfacial properties in composites, Compos. Sci. Technol. 68 (2008) 2042–2048.
[18] S. Kim, A. Faghihnejad, Y. Lee, Y. Jho, H. Zeng, D.S. Hwang, Cation–π interaction in DOPA-deficient mussel adhesive protein mfp-1, J. Mater. Chem. B 3 (2015) 738–743.
[19] S. Kim, H.Y. Yoo, J. Huang, Y. Lee, S. Park, Y. Park, S. Jin, Y.M. Jung, H. Zeng, D.S. Hwang, Salt triggers the simple coacervation of an underwater adhesive when cations meet aromatic π electrons in seawater, ACS Nano 11 (2017) 6764–6772.
[20] Y.-K. Kim, D.-H. Min, The structural influence of graphene oxide on its fragmentation during laser desorption/ionization mass spectrometry for efficient small molecule analysis, Chem. Eur J. 21 (2015) 7217–7223.
[21] M. Park, T. Lee, B.-S. Kim, Covalent functionalization based heteroatom doped graphene nanosheet as a metal-free electrocatalyst for oxygen reduction reaction, Nanoscale 5 (2013) 12255–12260.
[22] B. Delley, From molecules to solids with the DMol 3 approach, J. Chem. Phys. 113 (2000) 7756–7764.
[23] Y.A. Mankelevich, E.N. Voronina, T.V. Rakhimova, A.P. Palov, D.V. Lopaev, S.M. Zyryanov, M.R. Baklanov, Fluorine atoms interaction with the nanoporous materials: experiment and DFT simulation, Eur. Phys. J. D 71 (2017) 126.
[24] B.J. Yang, H. Shin, H.-K. Lee, H. Kim, A combined molecular dynamics/micromechanics/finite element approach for multiscale constitutive modeling of nanocomposites with interface effects, Appl. Phys. Lett. 103 (2013) 241903.
[25] K. Kim, Y.C. Jung, S.Y. Kim, B.J. Yang, J. Kim, Adhesion enhancement and damage protection for carbon fiber-reinforced polymer (CFRP) composites via silica particle coating, Composites Part A 109 (2018) 105–114.
[26] B.J. Yang, H. Shin, H. Kim, H.-K. Lee, Strain rate and adhesive energy dependent viscoplastic damage modeling for nanoparticulate composites: molecular dynamics and micromechanical simulations, Appl. Phys. Lett. 104 (2014) 101901.
[27] C. Park, B.J. Yang, K.B. Jeong, C.B. Kim, S. Lee, B.C. Ku, Signal-induced release of guests from a photolatent metal–phenolic supramolecular cage and its hybrid assemblies, Angew. Chem. Int. Ed. 56 (2017) 5485–5489.
[28] H. Sun, Z. Jin, C. Yang, R.L. Akkermans, S.H. Robertson, N.A. Spenley, S. Miller, S.M. Todd, COMPASS II: extended coverage for polymer and drug-like molecule databases, J. Mol. Model. 22 (2016) 47.
[29] S.Y. Kim, H.G. Jang, C.-M. Yang, B.J. Yang, Multiscale prediction of thermal conductivity for nanocomposites containing crumpled carbon nanofillers with interfacial characteristics, Compos. Sci. Technol. 155 (2018) 169–176.
[30] Y.-K. Kim, D.-H. Min, Simultaneous reduction and functionalization of graphene oxide by polyallylamine for nanocomposite formation, Carbon Lett. 13 (2012) 29–33.
[31] Y. Lin, Q. Liu, J. Fan, K. Liao, J. Xie, P. Liu, Y. Chen, Y. Min, Q. Xu, Highly dispersed palladium nanoparticles on poly(N1,N3-dimethylbenzimidazolium)iodide-functionalized multiwalled carbon nanotubes for ethanol oxidation in alkaline solution, RSC Adv. 6 (2016) 102582–102594.
[32] C.B. Kim, K.B. Jeong, B.J. Yang, J.W. Song, B.-C. Ku, S. Lee, S.K. Lee, C. Park, Facile supramolecular processing of carbon nanotubes and polymers for electromechanical sensors, Angew. Chem. Int. Ed. 56 (2017) 16180–16185.
[33] C. Lv, Q. Xue, D. Xia, M. Ma, J. Xie, H. Chen, Effect of chemisorption on the interfacial bonding characteristics of graphene− polymer composites, J. Phys. Chem. C 114 (2010) 6588–6594.
[34] S.-C. Shiu, J.-L. Tsai, Characterizing thermal and mechanical properties of graphene/epoxy nanocomposites, Composites Part B 56 (2014) 691–697.